Journal of Hepatocellular Carcinoma

Dovepress
Taylor & Francis Group

Open Access Full Text Article

ORIGINAL RESEARCH

Newly Established Anoikis-Associated Genes Predict the Prognosis of Hepatocellular Carcinoma

Yuyao Li[1,*], Er Li[2,*], Wenlan Zheng[1], Jia Shi[1], Shihan Yu[1], Xuemei Zhang[1], Liming Zheng[1], Wurong Du[1], Hao Liu[1], Hai Feng[2], Jianfeng Guo[3], Zhuo Yu[1]

[1]Department of Liver Disease, Shuguang Hospital Affiliated to Shanghai University of Traditional Chinese Medicine, Shanghai, 201203, People's Republic of China; [2]Institute of Infectious Disease, Shuguang Hospital Affiliated to Shanghai University of Traditional Chinese Medicine, Shanghai, 201203, People's Republic of China; [3]School of Pharmaceutical Sciences, Jilin University, Changchun, 130021, People's Republic of China

*These authors contributed equally to this work

Correspondence: Zhuo Yu; Jianfeng Guo, Email zhuoyu@shutcm.edu.cn; jguo@jlu.edu.cn

Objective: Anoikis is an anchorage-dependent programmed cell death implicated in multiple pathological processes of cancers; however, the prognostic value of anoikis-related genes (ANRGs) in hepatocellular carcinoma (HCC) remains unclear. Our study aims to develop an ANRGs-based prediction model to improve prognostic assessment in HCC patients.

Methods: The RNA-seq profile was performed to estimate the expression of ANRGs in HCC patients. The univariate Cox regression and the least absolute shrinkage and selection operator (LASSO) Cox regression analysis were applied in the model construction to predict the prognosis in terms of differentially expressed ANRGs in the Cancer Genome Atlas (TCGA) training cohort. The TCGA test cohort and the International Cancer Genome Consortium (ICGC)-originated cohort were set to verify the predictive capacity. Nomogram was built on the basis of risk score (RS), gender, age, grade, and T_stage, with the hope of extending the predictive ability of ANRGs to evaluate the HCC prognosis. The expression of differentially expressed ANRGs was assessed in HCC cell lines and orthotopic tumor-bearing mice.

Results: Six ANRGs (*ANXA5, BIRC5, BSG, DAP3, SKP2* and *CDKN3*) demonstrated the critical prognostic significance in HCC patients. The prognostic *RS* model on the basis of these ANRGs was capable of properly predicting 1-, 3-, and 5-year survivals. The Kaplan-Meier results displayed the increased death and decreased survival in the high-risk group. The *RS* acted as the independent factor for the survival evaluation. Our nomogram model was able to directly reflect the survival probabilities of each patient, which was confirmed through various validations. The transcription and translation of six ANRGs were significantly enhanced in HCC cell lines and tumor tissues.

Conclusion: Despite the lack of mechanistic validation, our anoikis-linked *RS* model serves as a promising tool for predicting HCC prognosis in clinical practice, and provides valuable insights into the decision of individualized therapeutic approaches.

Keywords: liver cancer, anoikis, tumor prognosis, risk model, nomogram, validation

Introduction

Hepatocellular carcinoma (HCC) remains the most commonly primary liver cancer, annually causing new morbidity and mortality over 670,000 and 620,000 worldwide.[1] HCC can be induced by different etiologies, such as hepatitis B virus and hepatitis C virus infections, obesity, diabetes mellitus, and alcohol abuse.[2] HCC development generally experiences liver injury, chronic inflammation, liver fibrosis, cirrhosis, and carcinogenesis.[3] Despite the great progression of therapeutic modalities, the prognosis of HCC is still poor, with the lower five-year survival rate.[4] Recent advancements in gene detection technologies, alongside a deepening understanding of molecular mechanisms, have facilitated improvements in both prognosis and therapeutic strategies for HCC.[5] Immunotherapy, in particular, represents a promising treatment approach. For example, studies have shown that ginsenoside Rh1 can upregulate MHC-I expression in MHC-I positive cells by

Received: 9 April 2025
Accepted: 21 August 2025
Published: 3 September 2025

suppressing the glucocorticoid receptor, thereby increasing the infiltration of $CD8^+$ T cells and mature dendritic cells.[6] Furthermore, immune checkpoint inhibitors (ICIs), such as antibodies targeting programmed cell death 1 (PD-1) or programmed death ligand 1 (PD-L1), have demonstrated significant success in the treatment of HCC and other cancers. Supporting this advancement, the immunoscore model, based on immune-related molecules, has been developed to predict therapeutic response to anti-PD-1 immunotherapy specifically in HCC patients.[7] Consequently, the robust predictive models constructed based on gene signatures are favorable to achieve the accurate judgment on the prognosis of HCC patients.[8–11]

Anoikis is the anchorage-dependent programmed cell death, which is caused through the cell detachment from the extracellular matrix (ECM).[12] Anoikis suppresses the cell attachment on the inappropriate ECM and therefore prevents the detached epithelial cells from colonizing the distant site.[13] Increasing evidence suggests that anoikis resistance is responsible for tumor development.[14] Indeed, it has been reported that the expression of pro-apoptosis proteins is frequently inhibited in HCC cells, causing the blockade of anoikis-related signaling pathways.[15] In addition, the anoikis resistance promotes the upregulation of the pro-survival factors, leading to intrahepatic spread and extrahepatic metastasis of tumor cells.[16]

Recently, several established risk score (RS) models based on anoikis-related genes (ANRGs) have demonstrated the potential for predicting the prognosis of diverse cancers.[17–20] However, ANRGs, which can fully achieve the prognostic prediction, are still deficient for HCC patients. In this study, we identified 6 differentially expressed ANRGs that were highly associated with the prognostic activities, demonstrating great potential for establishing a risk-predictive model to promote HCC management.

Materials and Methods

Data Collection and Process

The dataset of HCC patients (N=418) was selected and obtained in the Cancer Genome Atlas (TCGA) database (see a link in portal.gdc.cancer.gov/repository), and the RNA sequencing (RNA-seq) and clinical results were processed with the unified standardization.[21] The gene expression in malignant and adjacent normal tissues in HCC patients was classified and profiled by the "limma" package R software. In this present work, 403 clinical samples were assigned to either training or test cohorts via digital randomization. The inclusion criteria are to meet (1) histological confirmation of hepatocellular carcinoma, and (2) samples including the complete TNM stages. The exclusion criteria include (1) patient accompanied with the history of other malignant tumors, and (2) general clinical data, such as survival information, are incomplete. The transcriptome and clinical information of 232 tumor tissues were collected in the International Cancer Genome Consortium (ICGC) database, and were employed in the external validation (see the link in dcc.icgc.org/projects/LIRI-JP).

The TCGA and ICGC databases are publicly accessible repositories that contain data from patients who have provided informed consent. Consequently, researchers are allowed to freely download and utilize this data for research purposes, and the publication of findings derived from these data is permitted. Given that the data is already anonymized and consented for research use, the clinical research ethics committee of Shanghai University of Traditional Chinese Medicine has exempted this study from the need for ethical approval.

ANRG Analysis Between Healthy and Tumor Tissues

In total, 434 ANRGs (see the information in Supplementary Table 1) were acquired in the GeneCards database (see the link in www.genecards.org).[22] The "Limma" package R software ($|\log_2 FC|>1$, false discovery rate (FDR)<0.05) was applied for identifying differentially expressed genes (DEGs) in tumoral and adjacent non-tumroal tissues. The co-expressed relation and heatmap drawing of DEGs were described by means of "reshape2", "igraph", and "pheatmap" R software. The Search Tools for the Retrieval of Interacting Genes (STRING version11.0, see the link in string-db.org/) were utilized for plotting the protein/protein interaction (PPI) network.

Consensus Clustering

The clustering analysis was carried out to describe the relation of differentially expressed ANRGs and HCC subtypes. Patients were categorized to diverse clusters in terms of the "ConsensusClusterPlus" package, and the heatmap was plotted to display the clinical information and the differentially expressed ANRGs among these clusters. The KM analysis using the "survminer" R package was conducted to evaluate the difference of patient survival.

Establishment and Verification of ANRG-Related Prognostic Model

The univariate Cox regression analysis was performed in determining the prognostic role of differentially expressed ANRGs in the training cohort, with the purpose to screen candidates that have the significant relation to the overall survival (OS). The penalty parameter of the minimum standard was determined via the LASSO Cox regression analysis in "glmnet" R package. A formula of RS = $\Sigma X_i Y_i$ (X and Y separately represent the regression coefficient and the gene expression) was utilized to calculate the RS. Patients were split to low- and high-risk groups on a basis of the median RS. The OS times in two groups were evaluated through the KM analysis in the "Survminer" package. The principal component (PCA) and t-distributed stochastic neighbor embedding (t-SNE) analyses were performed using "Prcomp" package. A receiver operating curve (ROC) was built through the "time ROC" R package. The predictive potential of our prognostic model was validated by estimating the value of the area under the curve (AUC). Subsequently, to verify the applicability and superiority of the risk model, we used logistic regression, a traditional machine learning method, to construct a prognostic scoring system based on the six candidate genes and calculated the AUC value. The result shows that the risk model exhibits superior performance. TCGA test and ICGC-originated cohorts were also used to validate the reliability of the model. The levels of prognostic ANRGs were retrieved in the Gene Expression Profiling Interactive Analysis (GEPIA) (see the link in gepia.cancer-pku.cn).[23] The protein expressions of malignant and adjacent normal tissues were confirmed in the human protein atlas (HPA) database (see a link in www.proteinatlas.org).[24]

Independent Predictive Ability of ANRG-Related Prognostic Model

The univariate and multivariate Cox regression modalities were selected and applied for exploring the link between the ANRG-related prognostic model (in terms of the RS) and the clinicopathological factors.

Functional Enrichment and Analysis of Immune Cell Infiltration

To analyze the difference of gene function and signaling pathway between low- and high-risk groups, the "Limma" R package ($|\log_2 FC|>2$, FDR<0.05, set as significant difference) was carried out to identify the DEG expression. The "clusterProfiler" R package was selected and applied in the analysis of Gene ontology (GO) and Kyoto Encyclopedia of Gene and Genomes (KEGG). The "CIBERSORT" R package was set for depicting tumor immune microenvironment.

Construction and Validation of Nomogram

Using the "rms" R package, a Nomogram was constructed in term of the *RS* of HCC patients, derived from the ANRG formula, and the clinical characteristics such as age, gender, grade and T_stage. The corresponding 1-, 3- and 5-year survival probabilities were evaluated according to the scores of each patient. The calibration, KM, and ROC curves were developed using "rms", "Survminer", and "Time ROC" R packages, respectively, with the purpose to determine the predictive accuracy of Nomogram. In addition, the TCGA test and ICGC-originated external validation cohorts were used to verify the reliability of Nomogram.

Cell Culture and HCC Mouse Model

The cell lines used in this experiment were mouse HCC cell line Hepa1-6, human HCC cell line Huh7, and human normal hepatic cell line HL-7702, derived from the American Typical Culture Collection Center (ATCC). All cells were inoculated in DMEM medium supplemented with 10% fetal bovine serum, 100 U/L penicillin, and 100 mg/L streptomycin, and cultured in the cell incubator at 37°C, and 5% CO_2.

5-week-old male C57BL/6 mice were obtained from the SLAC Laboratory Animal Company. Following established protocol previously described, 5×10^6 of Hepa1-6 cells were injected into the liver lobe to create the orthotopic HCC model, as compared to the control group.[25]

The study design was reviewed and approved by the Animal Experimentation Ethics Committee of Shanghai University of Traditional Chinese Medicine. All animal experiments were conducted in accordance with the "Helsinki" Declaration for the welfare of the laboratory animals.

Quantitative RT-PCR

Total RNAs were extracted using the Trizol agent (Invitrogen) and subsequently quantified. These RNA samples were then reverse transcribed into cDNAs. The cDNAs corresponding to the genes *ANXA5, BIRC5, BSG, DAP3, SKP2* and *CDKN3* were amplified using a real-time fluorescent quantitative PCR kit. The transcription levels of these genes were measured and normalized against *GAPDH* that served as the loading control. The specific primer sequences used for amplification were shown in the Supplementary Table 2.

Immunohistochemistry

Tissue samples obtained from the mice were treated with formalin, embedded with paraffin, dehydrated, and sliced to the 5-μm sections. These sections were subsequently deparaffinized, rehydrated, and washed. For antigen retrieval, the sections were boiled in the citrate repair solution (pH=6.0) for half an hour, and endogenous peroxidase activity was deactivated for ten minutes. The sections were then incubated with primary antibodies, including anti-mouse ANXA5 (ab108321; 1:100), anti-mouse BIRC5 (ab76424; 1:1000), anti-mouse BSG (ab108308; 1:3000), anti-mouse DAP3 (ab302889; 1:100), anti-mouse SKP2 (ab183039; 1:50), and anti-mouse CDKN3 (Invitrogen PA5-120764; 1:100). Finally, the sections were incubated with secondary antibodies before the analysis.

Statistical Analysis

The transcriptomic data and clinical information were analyzed using R software (v4.1.0). The integration and acquisition of transcriptomic data were executed by Perl language. The DEGs in normal and tumor samples were analyzed using one-way analysis of variance test. The KM method and the log-rank Mantel-Cox test were utilized in the OS determination. The univariate and multivariate Cox regression modalities were utilized to estimate the independent prognostic value. The Cox risk proportional regression modality was performed to determine the prognostic factor with risk ratio and 95% confidence interval (CI). The GraphPad Prism8 software was selected for data analysis and image process. Results were shown as mean ± SEM.

Results

Most ANRGs Show Increased Expression in HCC Tissues

In this study, 101 DEGs were identified by assessing the transcription level of ANRGs in 31 adjacent normal tissues and 355 malignant tissues in the TCGA database. Top 50 genes with the significant ($P<0.05$) changes in their RNA level were selected according to the setting of |Log2FC|>1, and most of them are at higher level in HCC tissues than in normal ones (Figure 1A). In addition, when exploring the interaction of the genes with anoikis, PPI analysis was carried out in a setting of the minimum interaction score of 0.9 with the best confidence. Accordingly, *ITGB1, ITGA2, ITGB4, PTK2, BSG, HGF*, and *SRC* were confirmed as the hub genes (Figure 1B). The link of these genes was exhibited in Figure 1C.

Consensus Clustering Analysis Divides HCC Patients Into Two Clusters with Different Clinical Characteristics

In order to reveal the connection of differentially expressed ANRGs with the clinical characters, the consensus clustering analysis was performed for stratifying the patients with HCC in the TCGA dataset. By testing the clustering variable (k) from two to nine, patients were optimally classified into two clusters (k=2), exhibiting the lowest intergroup correlation and the highest intragroup correlation (Figure 2A). The heatmap displayed gene expression profiles and clinical

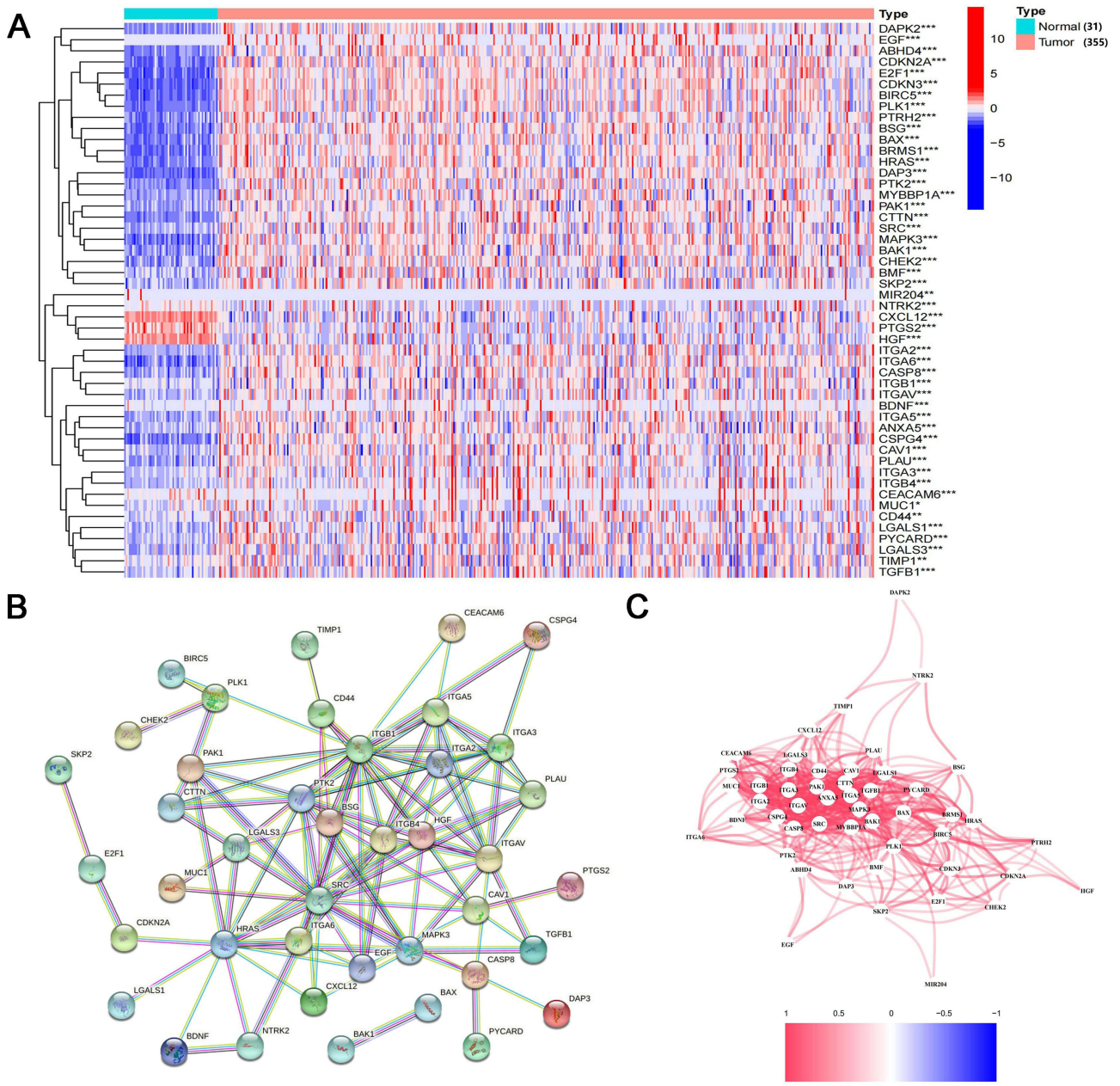

Figure 1 Expression levels and mutual interactions of ANRGs. (**A**) A heatmap showed the levels of the top 50 ANRGs with significant expression change between normal tissues (N, blue) and tumor tissues (T, red). **P*<0.05; ***P*<0.01; ****P*<0.001. (**B**) A PPT network displayed the interactions of ANRGs. (**C**) The correlation network of the ANRGs was constructed. (Red line, positive correlation).

characters in two clusters, including metastasis (N, M, and T sub-phases), stage (stage I–IV), differentiation (G1-4), gender, and age (over or less 65 years). The Pearson Chi-square test was utilized for assessing the difference among these characters of two clusters (Figure 2B), indicating the significance in age (P<0.05) and tumor differentiation (P<0.001). When the OS was evaluated in two clusters (Figure 2C), cluster 1 displayed the advantage with statistical significance (P<0.001) in the long survival condition over cluster 2.

Specific ANRGs are Selected to Construct Prognostic Risk Model

In the TCGA database, 403 HCC samples were matched to patients with complete survival information. They were split into the training and test cohorts using the digital randomization method, and the clinical characteristics between two

https://doi.org/10.2147/JHC.S533398

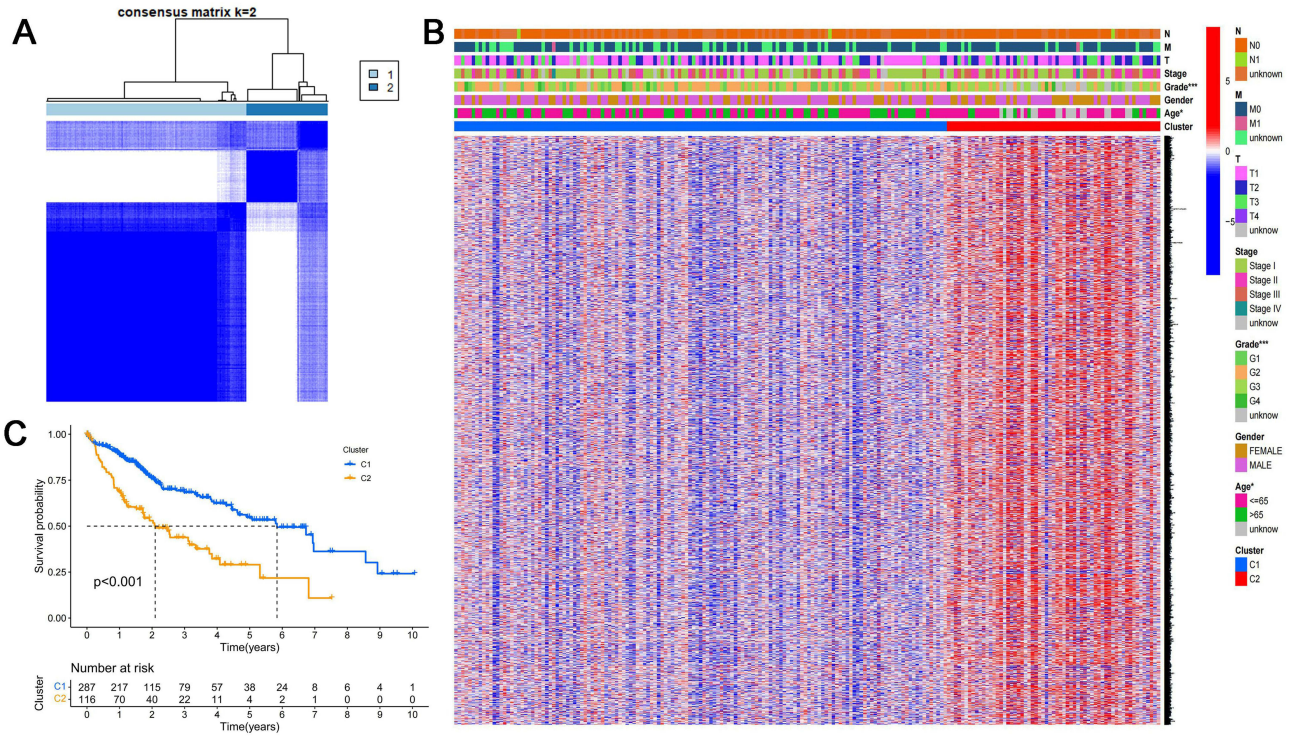

Figure 2 Classification of HCC cases based on DEGs. (**A**) HCC cases were separated into two clusters in the consensus clustering matrix in the condition of k=2. (**B**) A heatmap showed the gene expression profile concomitant with clinical pathological characteristics in the two clusters. The color coding used to represent these characteristics are as follows: Clinical Stage I, gray-green; Stage II, rose-red; Stage III, brick-red; Stage IV, deep green; Unknown, silver-gray. Pathological Grade I, tender green; Grade II, Orange; Grade III, yellow-green; Grade IV, grass green; Unknown, silver-gray. (**C**) The comparison of OS in the two clusters was shown in Kaplan–Meier survival curves. *P<0.05; ***P<0.001.

cohorts showed no significant difference (Supplementary Table 3). When DEGs were evaluated by the univariate cox regression modality in training cohort, 10 candidate prognosis-related ANRGs were screened (Figure 3A). Six prognostic signatures (*ANXA5, BIRC5, BSG, DAP3, SKP2* and *CDKN3*) were then identified via the LASSO Cox regression modality. Moreover, the risk model was established at the optimum λ value (Figure 3B and C). *RS* = (0.0071×*ANXA5* exp.) + (0.0465×*BIRC5* exp.) + (0.0164×*BSG* exp.) + (0.0574×*DAP3* exp.) + (0.0646×*SKP2* exp.) + (−0.0195×*CDKN3* exp.).

The *RS* was calculated and arrayed in order, and the 202 HCC patients in training cohort were categorized in low- and high-risk groups by the median *RS* (Figure 3D). Patients well corresponded to low- and high-risk groups, as confirmed by the T-distributed stochastic neighbor embedding (t-SNE) analysis and the principal component analysis (PCA) (Figure 3E and F). In comparison to the results recorded by the low-risk group, the higher mortality and shorter survival were shown by the high-risk group (Figure 3G). Two groups showed the profound difference (P=0.012) in the total survival via the KM analysis (Figure 3H). The time-dependent ROC analysis was conducted for evaluating the sensitivity and specificity of prognostic model, indicating that the AUC at 1, 3, and 5 years was 0.731, 0.660, and 0.669, respectively (Figure 3I). In addition, to validate the applicability and the superiority of the risk model, we conducted ROC analysis using a traditional model with an AUC value of 0.651. Therefore, compared with the traditional dichotomous model, logistic regression showed that the risk model performs better in predicting the survival status of patients (Figure S1).

Internal and External Validation of Prognostic Risk Model

Next, TCGA Test and ICGC-originated cohorts were applied to corroborate the validity of prognostic model. Two cohorts were split in low- and high-risk groups in terms of the median *RS* obtained in TCGA training cohort (Figure S2A and B). PCA and t-SNE analyses demonstrated that patients with diverse *RS* have been well assigned into two groups in both the TCGA test and ICGC-originated cohorts (Figure S2C–F). The high-risk group exhibited significantly higher death rates

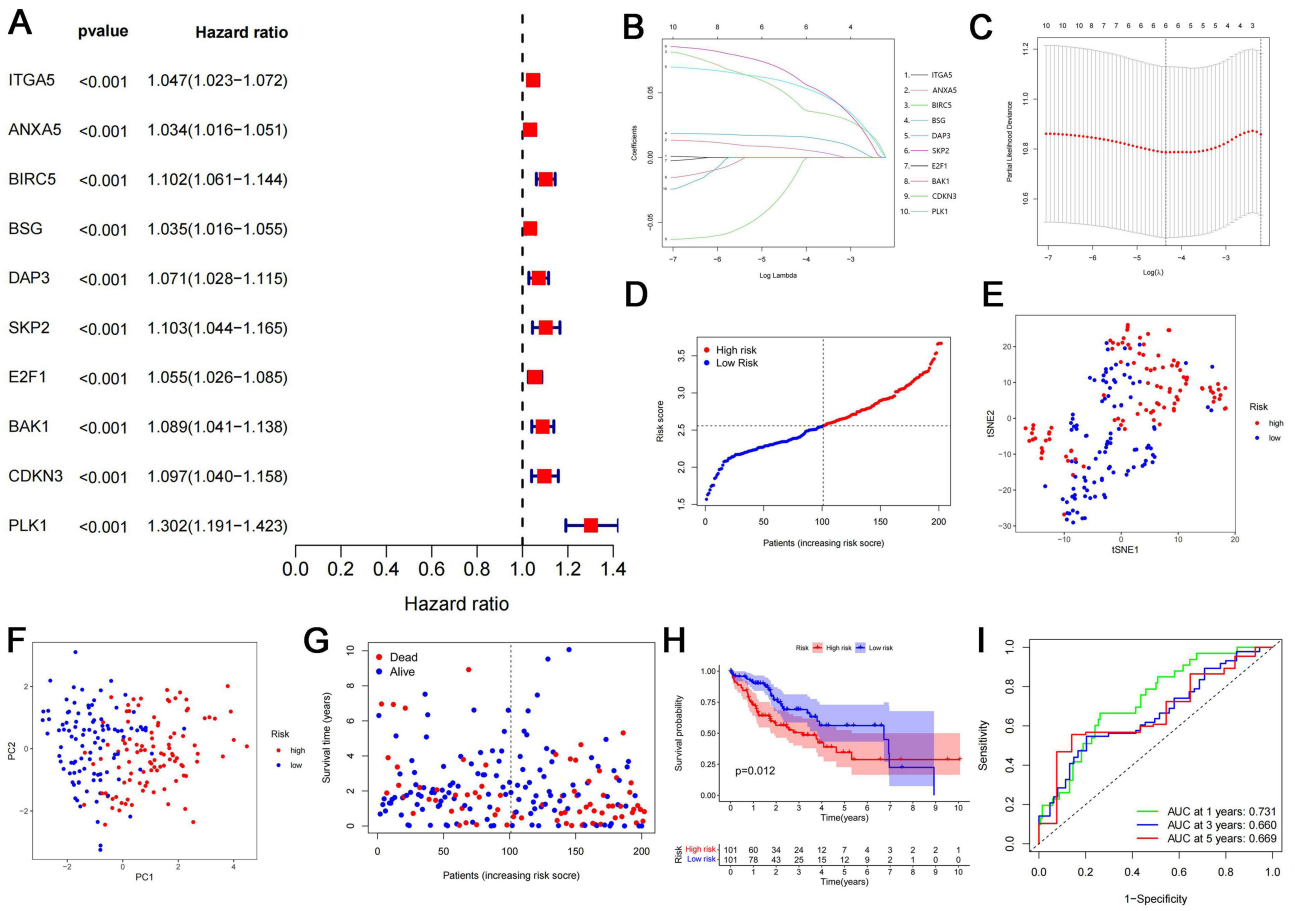

Figure 3 Construction of ANRG-related prognosis model in TCGA training cohort. (**A**) A total of 10 ANRGs were identified with significant difference in the training cohort via the univariate Cox regression analysis (P<0.05). (**B**) LASSO Cox regression was performed to assess the 10 ANRGs for the construction of a prognosis model. (**C**) The 10 ANRGs were under the cross validation for tuning parameter selection in LASSO regression. (**D**) Patients in the training cohort were aligned in order of risk score. (**E**) Survival condition of HCC patients was displayed in T-SNE based on the risk score. (**F**) Survival condition of HCC patients was displayed in PCA based on risk score. (**G**) Survival condition of each patient was shown in two groups (low-risk group: left side of the dotted line; high-risk group: right side of the dotted line). (**H**) The survival condition of patients in high- and low-risk group were analyzed by Kaplan-Meier survival curves. (**I**) The predictive effect of the prognostic model was assessed by ROC curve.

and shorter survival periods compared to the low-risk group (Figure S2G and H). The KM analysis revealed that the OS in the low-risk group was significantly longer in either TCGA test or ICGC-originated cohorts, with statistical significance at $P<0.001$ and $P=0.005$, respectively (Figure S2I and J). The model reliability was also verified using the ROC analysis (Figure S2K and L). As demonstrated in Figure S2K, AUC at 1 year, 3 years, and 5 years at TCGA test cohort was 0.755, 0.747, and 0.659. As demonstrated in Figure S2L, AUC for 1-, 3-, and 5-year survivals at ICGC-originated cohort was 0.716, 0.669, and 0.677. These data confirm the reliability of our prognostic risk model.

Risk Score Is Validated to Be Independent Factor in the Prognostic Analysis

Apart from investigating the relevance of *RS* and clinical profile in HCC patients, we explored whether *RS* was the independent factor in predicting the OS of the cohorts. The univariate Cox regression modality illustrated that *RS* was a statistically significant independent prognostic factor for assessing patient survival in both the training cohort ($P<0.001$; HR=3.703, 95% CI: 2.042–6.713; Figure 4A) and test cohort ($P<0.001$; HR=3.390, 95% CI: 1.899–6.053; Figure 4B). By adjusting various confounding variables, the multivariate Cox regression modality also confirmed the role of *RS* as an independent prognostic factor, demonstrating a significant positive correlation between *RS* and poor survival outcomes in both the training cohort ($P<0.001$; HR=3.562, 95% CI: 1.946–6.521; Figure 4C) and test cohort ($P<0.001$; HR=2.887, 95% CI: 1.608–5.182; Figure 4D). Furthermore, the heatmap, integrating differentially expressed ANRGs and clinical

https://doi.org/10.2147/JHC.S533398

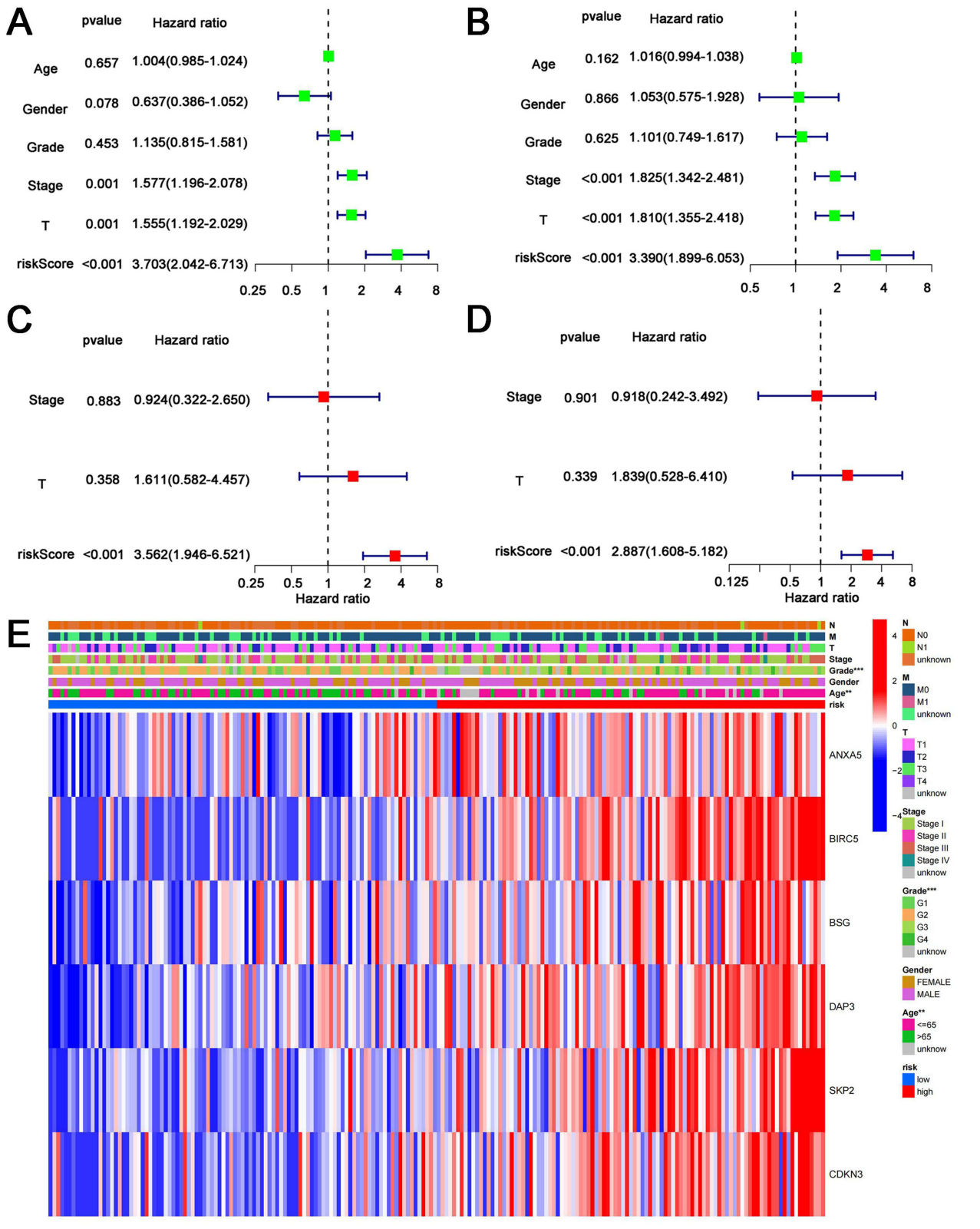

Figure 4 Independent prognostic value of prognostic risk model for HCC. (**A** and **B**) Univariate and multivariate Cox regression analysis of TCGA training cohort. (**C** and **D**) Univariate and multivariate Cox regression analysis of TCGA test cohort. (**E**) Heatmap displayed the relationship between the expression of DEGs and clinical characters. ***P*<0.01; ****P*<0.001.

characteristics, showed significant differences in age ($P<0.05$) and tumor grade ($P<0.001$) between low- and high-risk groups (Figure 4E).

Functional Analysis in Low- and High-Risk Groups

Next, DEGs were extracted from the training cohort using the "limma" R software ($|\log_2 Fc|\geq 1$, FDR<0.05), and gene functions and signaling pathways were analyzed in low- and high-risk groups clustered by our prognostic model. The analyses of GO and KEGG were conducted for evaluating the classification and function of DEGs. In the set of biological process, DEGs were concentrated on ribonucleoprotein complex biogenesis, RNA splicing, and protein targeting; in the set of cellular components, DEGs were enriched in cell-substrate junction, focal adhesion, and vesicle lumen; in the set of molecular functions (MF), cadherin binding, transcription coregulatory activity and ubiquitin-like protein ligase binding were highly linked to DEGs (Figure 5A). The KEGG analysis showed that the ribosome and carbon metabolism and the COVID-19 course were the top signaling pathways enriched by DEGs (Figure 5B).

Analysis of Immune Cell Infiltration in HCC Cohorts

To explore the relationship between immune cell infiltration and survival outcomes, in HCC cohorts, we employed the CIBERSORT algorithm to analyze immune cell profiles in both low- and high-risk groups. Twenty-two sets of immune cells were found to accumulate in both tumor and normal tissues across the training and test cohorts (Figure 6A–D). Notably, there was a significant difference in the infiltration of resting memory $CD4^+$ T cells and monocytes, which were more prevalent in the low-risk group compared to the high-risk group. In contrast, follicular T helper cells and M0 macrophages were significantly more abundant in the high-risk group than in the low-risk group (Figure 6E and F). These findings suggest a differential pattern of immune cell infiltration associated with risk stratification in HCC, which may have implications for understanding the tumor microenvironment and its impact on patient survival.

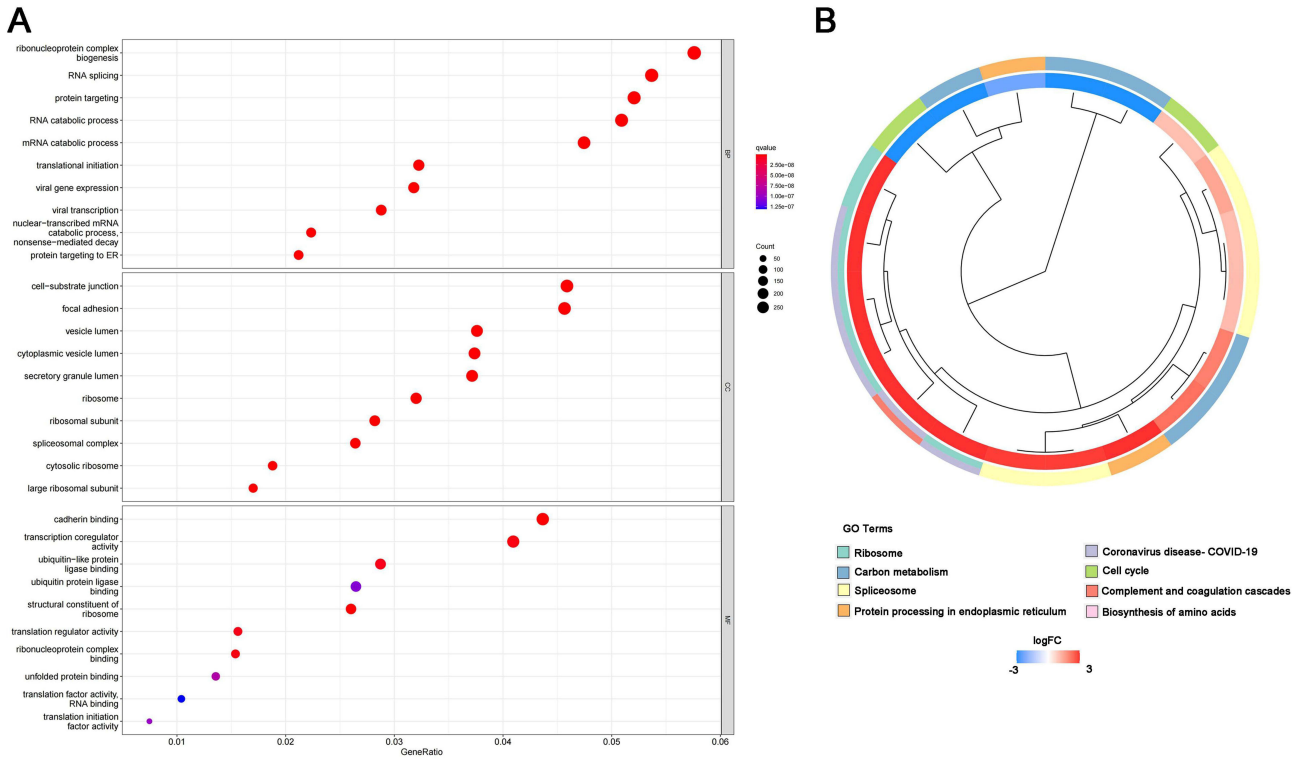

Figure 5 Analysis of gene function in high and low-risk groups. (**A**) Bubble diagram of GO enrichment (the larger the bubble, the more genes are enriched; and the increasing depth of red, the more obvious the difference). (**B**) Circle plot through KEGG analysis visualizing the signaling pathways enriched by DEGs.

https://doi.org/10.2147/JHC.S533398

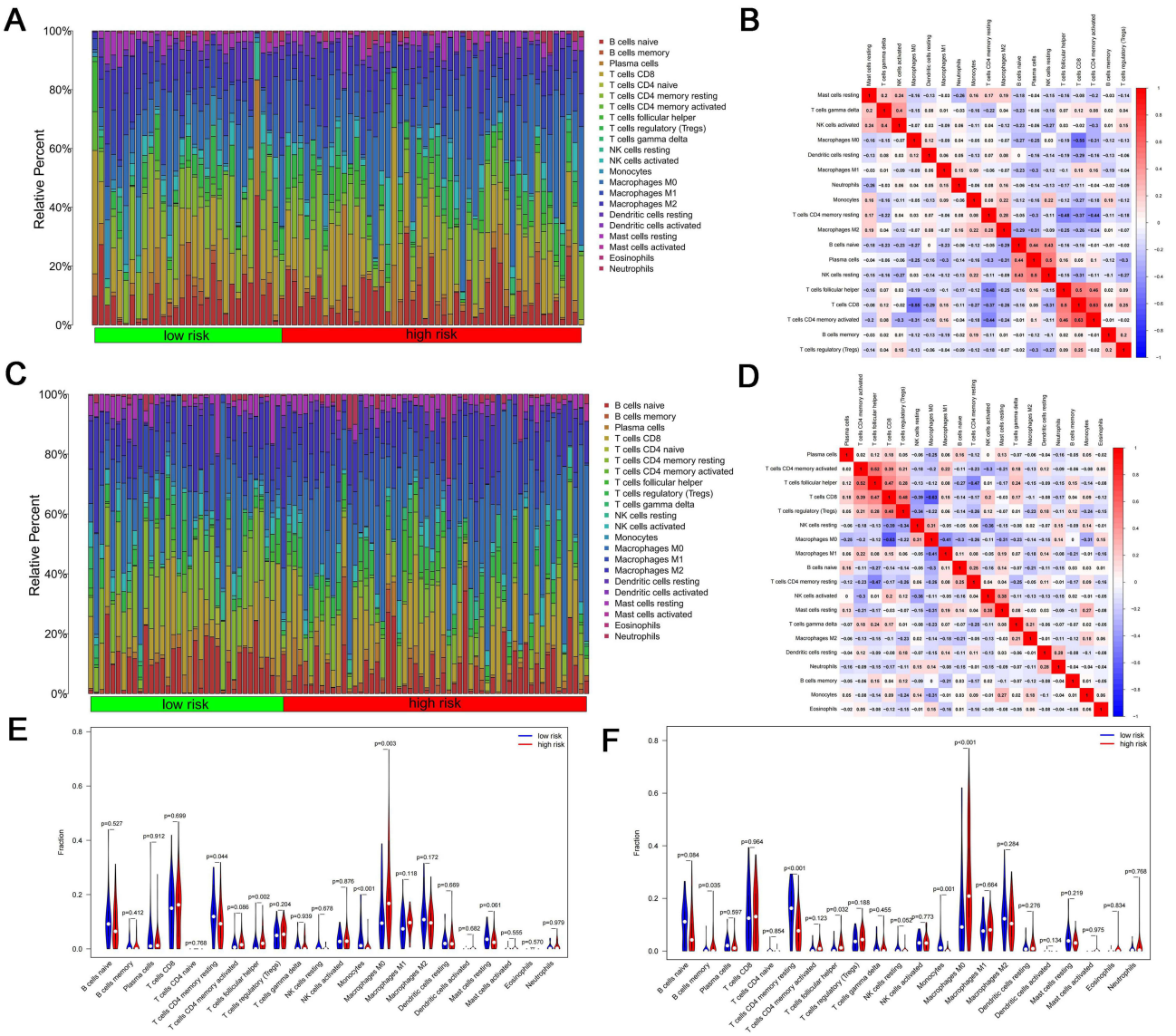

Figure 6 Analysis of immune cell infiltration in HCC cohort. (**A** and **C**) Histogram of different immune cell contents in the TCGA training cohort and test cohort. (**B** and **D**) Correlation between immune cells. Red represented positive correlation genes and blue represented negative correlation genes. Point size represented *P* value. X axis and Y axis indicated immune cell type. (**E** and **F**) Violin diagram showed the difference of content of each immune cell in high- and low-risk group in the TCGA training cohort and test cohort. (Red, high expression; green, low expression.).

Nomogram Construction to Predict the Survival

A nomogram was developed to enhance prognostic prediction by utilizing clinical characteristics obtained from the TCGA database and the HCC training cohort, excluding patients with missing information. This nomogram classified patients based on percentage survival coefficients (1-, 3-, and 5-year) derived from the cumulative information scores of relevant clinical characteristics (Figure 7A). Calibration curves demonstrated that the nomogram's predictions closely aligned with actual observed probabilities (Figure 7B–D). Furthermore, the KM curve indicated that the mean survival time was significantly shorter for patients in the high Nomo-risk group compared to those in the low Nomo-risk group ($P = 0.00016$, Figure 7E). The AUCs for the ROC curves were 0.806 for 1-year, 0.729 for 3-year, and 0.800 for 5-year predictions, confirming the nomogram's precision (Figure 7F). Additionally, the effectiveness of the nomogram was validated through decision curve analysis (DCA) (Figure 7G).

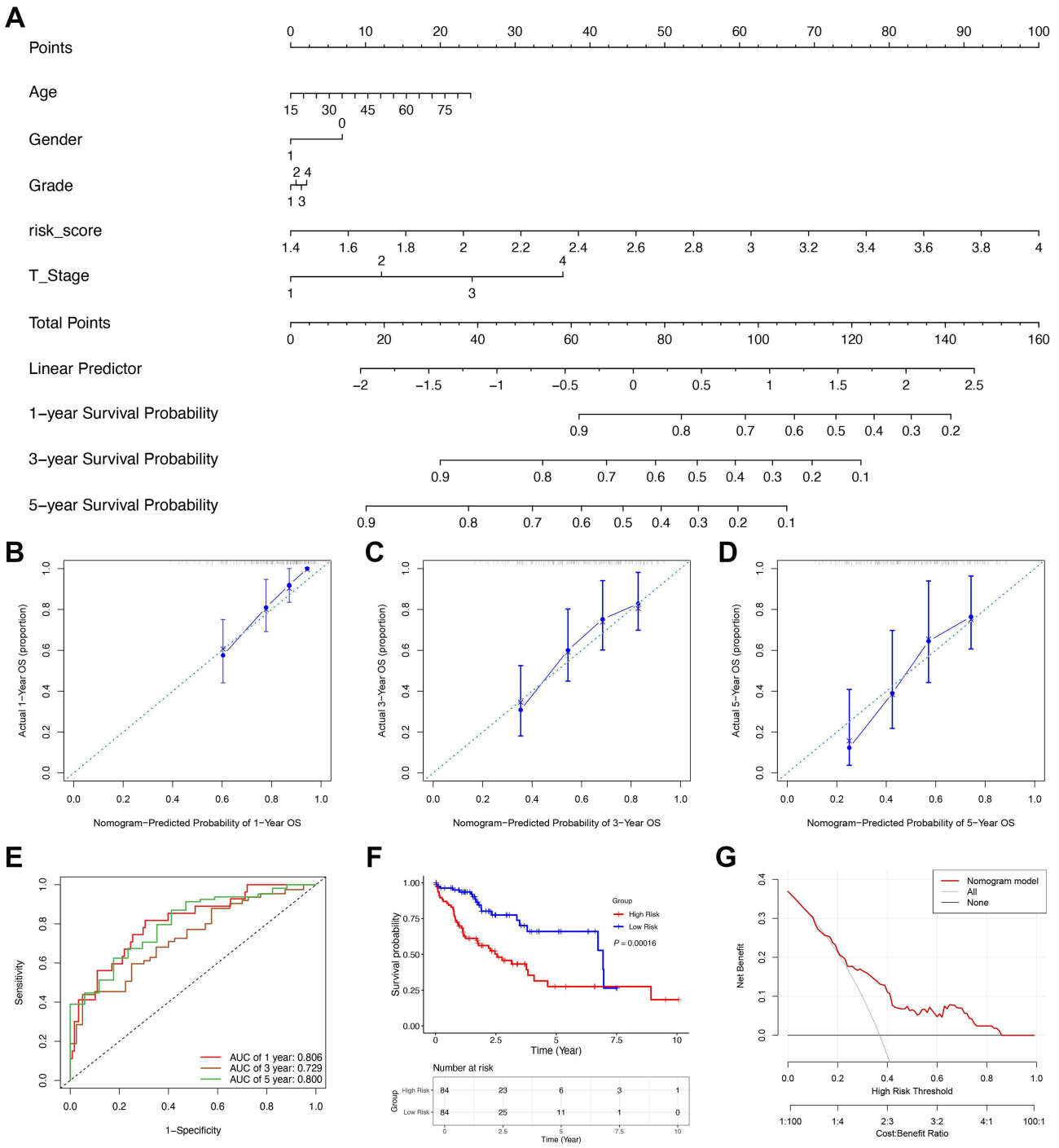

Figure 7 Nomogram construction and TCGA internal training cohort validation. (**A**) Histograms predicting 1-, 3-, and 5-year overall survival in patients with HCC. (**B**–**D**) Calibration curves for survival outcome prediction. (**E**) Receiver Operating Characteristic (ROC) Curves for Nomogram's 1-, 3-, and 5-year overall survival. (**F**) Kaplan-Meier (KM) curves between Nomogram risk groups. (**G**) Decision Curves Analysis (DCA) to analyze the clinical value of nomogram.

Internal and External Validation of Nomogram

The validity of the Nomogram was corroborated using cohorts derived from the TCGA test and ICGC. In the TCGA internal test cohort, the Nomogram demonstrated the accuracy in predicting OS for HCC patients, as evidenced by the AUC values of 0.799 at 1-year, 0.761 at 3-year, and 0.697 at 5-year (Figure S3A). The KM curves further illustrated that the mean survival time was significantly shorter in the high Nomo-risk group compared to the low Nomo-risk group (P = 0.00016; Figure S3B). Additionally, DCA indicated the clinical utility of the Nomogram (Figure S3C). Similarly, in the

ICGC-originated cohort, the Nomogram maintained AUC values exceeding 0.6, specifically 0.839 at 1-year, 0.797 at 3-year, and 0.699 at 5-year (Figure S3D). The KM curves for this cohort also showed a significantly shorter mean survival time for the high Nomo-risk group compared to the low Nomo-risk group ($P < 0.0001$; Figure S3E). The DCA results further supported the clinical value of the Nomogram (Figure S3F). Collectively, these findings confirm the robust performance and significant predictive value of the Nomogram in forecasting OS for HCC patients.

The mRNA Level and Protein Expression of Specific ANRGs Were Significantly Upregulated in Tumor Samples

The expression levels of six DEGs were investigated to validate ANRG expression in both normal and tumor samples. Initially, transcriptional analysis using the GEPIA database revealed that the mRNA levels of these DEGs were significantly elevated in tumor samples compared to normal tissues (Figure 8A). Complementary to this, protein expression analysis using the HPA database indicated a significantly higher protein level in tumor tissues relative to normal tissues (Figure 8B).

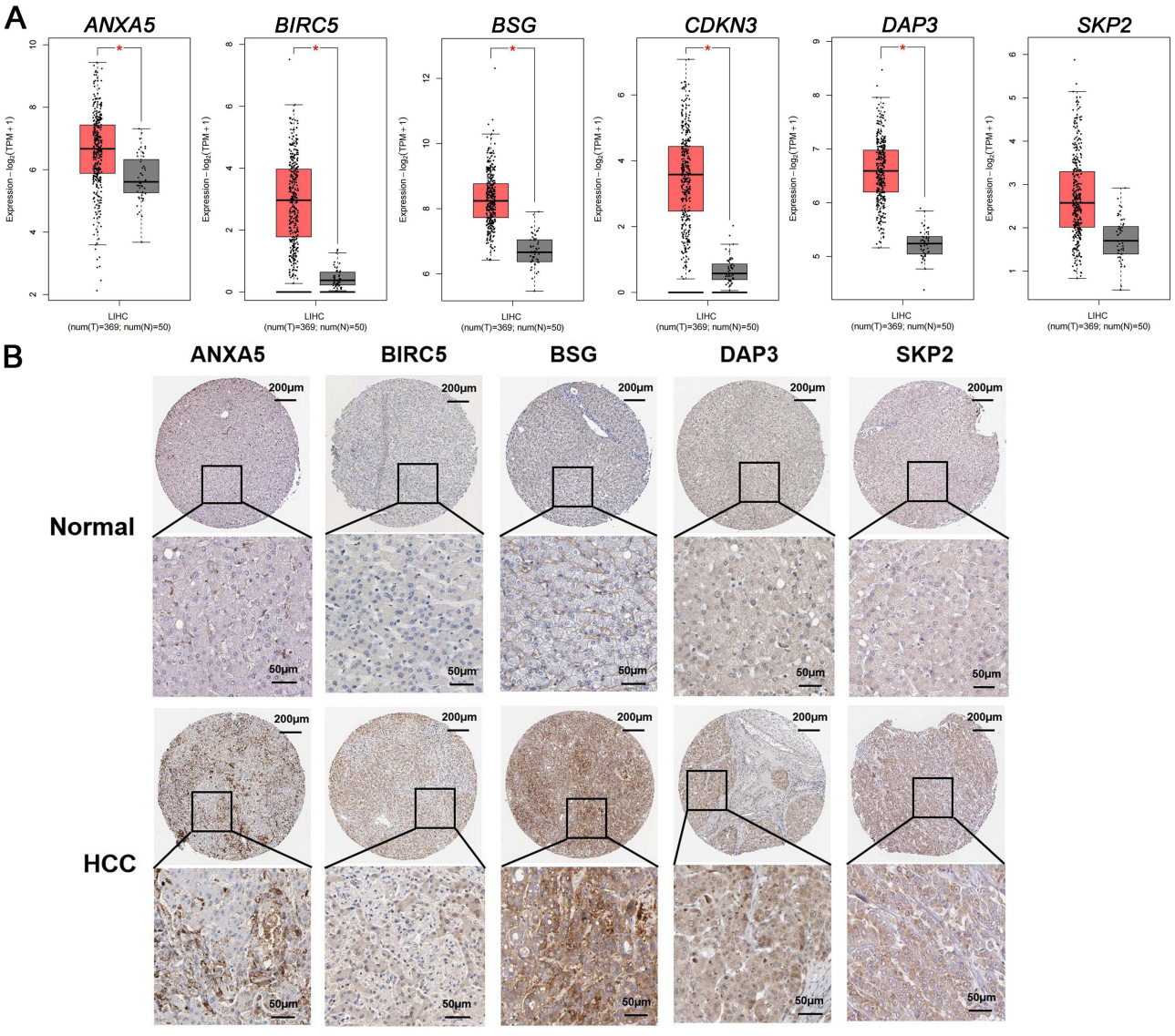

Figure 8 Validation of the ANRGs expression in the GEPIA database and HPA database. (**A**) The mRNA levels of *ANXA5, BIRC5, BSG, DAP3, SKP2* and *CDKN3* between normal and HCC tissues in the GEPIA, **P*<0.05. (**B**) Immunohistochemistry of the ANXA5, BIRC5, BSG, DAP3, SKP2 and CDKN3 were detected in normal and HCC tissues from the HPA database.

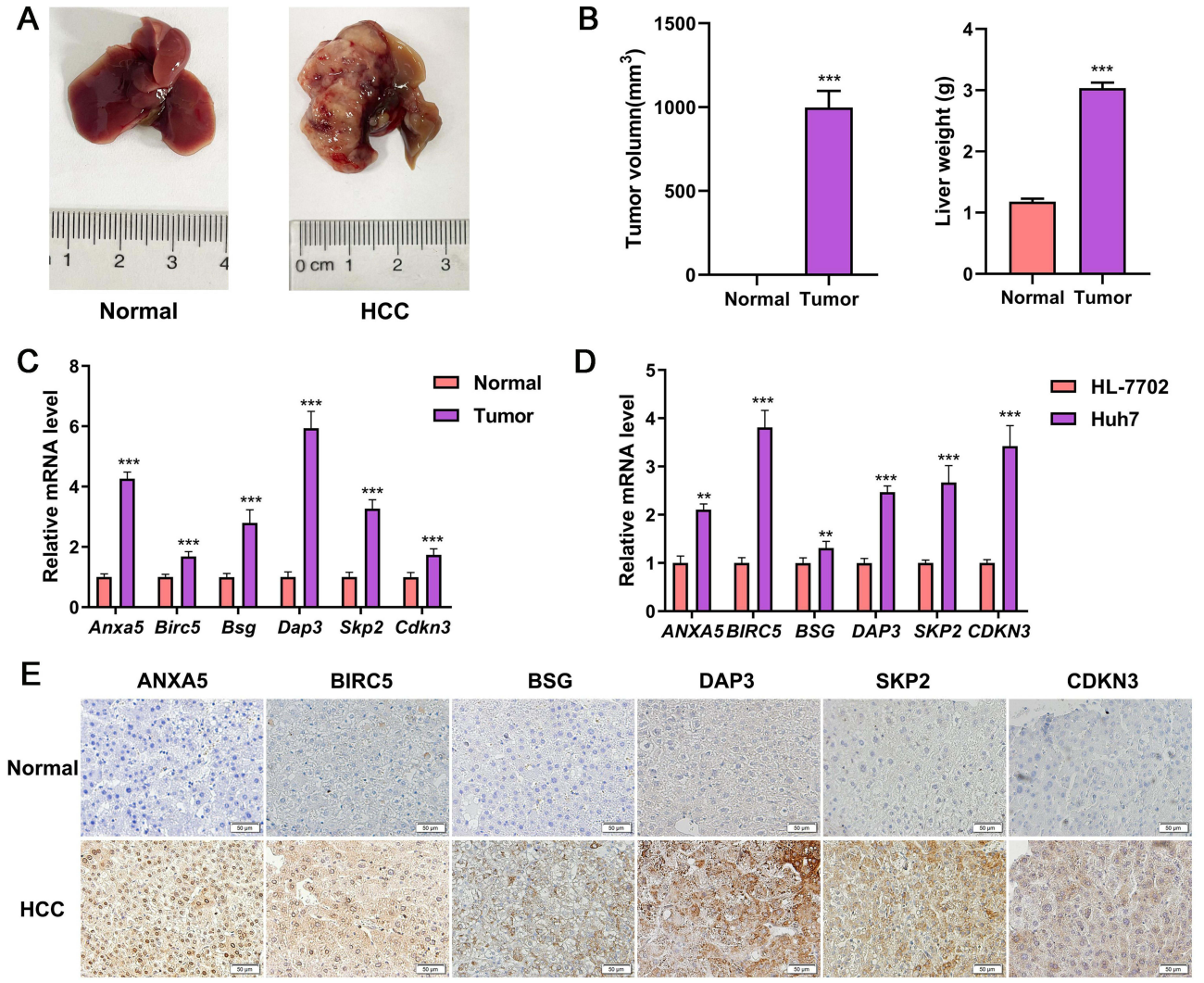

Figure 9 Validation of the ANRGs expression in vivo and in vitro. (**A**) Typical diagrams of normal and tumor liver tissue from mice were presented. (**B**) Tumor volumes and liver weight between normal and HCC models from mice (n=5, per group). (**C**) The mRNA levels of *ANXA5, BIRC5, BSG, DAP3, SKP2* and *CDKN3* were determined in the normal and HCC livers of mice (n=5 per group). (**D**) The mRNA levels of *ANXA5, BIRC5, BSG, DAP3, SKP2* and *CDKN3* between HL-7702 and Huh7 cells (n=3). ***P*<0.01; ****P*<0.001. (**E**) Immunohistochemistry showed that the expression of ANXA5, BIRC5, BSG, DAP3, SKP2 and CDKN3 in HCC tissues and non-tumor tissues from human samples.

Further validation was conducted through in vivo and in vitro experiments. Tumor growth was induced by inoculating Hepa1-6 cells into the liver, where a marked increase in the mRNA levels of ANRGs was observed in tumor tissues compared to normal liver tissues (Figure 9A–C). Additionally, in vitro analysis demonstrated that the mRNA levels of the six ANRGs were significantly elevated in Huh7 cells compared to HL-7702 cells (Figure 9D). Immunohistochemical evaluation further confirmed that the protein levels of ANRGs were significantly upregulated in the tumor tissues of HCC patients (Figure 9E). These findings collectively underscore the heightened expression of ANRGs in tumor samples, both at the transcriptional and translational levels, thereby reinforcing their potential role in tumorigenesis.

Discussion

Despite substantial advances in HCC therapy, the five-year survival rates remain low, primarily due to poor prognosis.[26] Anoikis, a form of programmed cell death that is dependent on cell anchorage, plays a crucial role in preventing the colonization of cells in inappropriate location.[27] Accumulating studies indicate that the failure of anoikis in cancer cells is closely linked to tumor growth and metastasis, including HCC.[28] Although several *RS* models have been developed based

on anoikis-related gene signatures in recent years, there remains a deficiency in ANRGs that can fully predict the prognosis of HCC.[29–32]

In this study, six differentially expressed ANRGs (*ANXA5, BIRC5, BSG, DAP3, SKP2* and *CDKN3*) were identified in HCC and normal tissues, and these genes were found to be closely linked to the prognosis of HCC treatment. To leverage this association, a prognostic *RS* model was developed using univariate Cox and LASSO Cox regression analyses based on these DEGs. This model demonstrated a robust capacity for predicting patient survival, and was able to independently assess the risk for patients in both TCGA and ICGC cohorts. Additionally, GO enrichment and KEGG pathway analyses were conducted to further profile the ANRGs. These analyses revealed that the genes were significantly associated with ribonucleoprotein complex biogenesis, cell-substrate junction, and cadherin binding. Moreover, they were highly enriched in signaling pathways related to the ribosome, carbon metabolism and the coronavirus disease COVID-19.

The involvement of immune cells within tumors is crucial for tumor initiation, development, metastasis, and therapy resistance.[33] Among these immune cells, $CD4^+$ T cells are particularly significant, acting as key coordinators of both innate and antigen-specific immune responses.[34] Recent studies have further highlighted the role of $CD4^+$ T cells as anti-tumor effector cells.[35] Consequently, an increased recruitment of resting memory $CD4^+$ T cells is associated with a better prognosis in low-risk groups. In contrast, macrophages in their resting or naïve state (M0), which originate from the bone marrow, have the potential to polarize into either pro-inflammatory (M1) or anti-inflammatory (M2) states in response to various stimuli.[36] Notably, a high infiltration of M0 macrophages has been closely linked to the poor OS in patients with HCC.[37,38] Thus, the presence of M0 macrophages in high-risk groups may indicate an unfavorable prognosis.

Monocyte subpopulations are known to perform distinct functions that can either promote or inhibit tumor immune responses.[39] Similarly, follicular T helper cells, which are essential for support to B cells in generating antibody-mediated immune activities, may also exhibit pro- or anti-tumor roles depending on the type of cancer involved.[40–42] Consequently, the potential of monocytes and follicular T helper cells, along with their subtypes, as predictive markers for HCC prognosis requires further investigation in future studies.

Annexin A5 (ANXA5) is a member of the calcium-dependent phospholipid binding protein family, typically found in the cytoplasm.[43] The protein encoded by *ANXA5* serves as an endogenous regulator in various physiological processes, including cell signal transduction, inflammation, tumor proliferation, metastasis, and therapy resistance.[44–46] Mechanistically, research indicates that ANXA5 can facilitate the malignant transformation of murine liver cancer Hca-F cells by activating the ERK2/c-Jun/pc-Jun (Ser73) and ERK2/E-cadherin pathways,[47] suggesting its involvement in metastasis, particularly lymph node metastasis (LNM).[48] Baculoviral inhibitor of apoptosis repeat-containing protein 5 (BIRC5) is a key gene encoding the inhibitor of apoptosis protein family, playing a significant role in suppressing apoptosis. BIRC5 is highly expressed in various cancers, contributing to malignant metastasis and recurrence, which are associated with patient prognosis.[49,50] For instance, the transcriptomic analyses of circulating tumor cells have shown that BIRC5, the key regulator of anoikis, can be upregulated during the dissemination of pancreatic ductal adenocarcinoma.[51] Mechanistically, BIRC5 functions to promote HCC cell proliferation by inhibiting apoptosis and promoting G2/M cell cycle transition, while knockdown of BIRC5 in HepG2 cells leads to decreased proliferation by disrupting cell division. Furthermore, BIRC5 deletion inhibits epithelial-mesenchymal transition (EMT) and reduces the levels of AURKA and CDK1/2, ultimately suppressing cell migration.[52] Basigin (BSG), a glycosylated transmembrane protein widely distributed on the cell surface, is instrumental in cell-cell interaction and ECM attachment.[53] Recent studies have reported that BSG is largely expressed in different cancers, promoting malignant invasion by inducing the release of matrix metalloproteinases from mesenchymal cells within the tumors.[54] Other studies indicated that lncRNA BSG-AS1 stabilized BSG mRNA, leading to increased BSG expression. This promotes HCC proliferation and migration, making high levels of poor HCC prognosis.[55] Death-associated protein 3 (DAP3), a member of the death-associated protein (DAP) family, is linked to mitochondrial morphological changes during apoptosis.[56] Functionally, DAP3 has been shown to stimulate cancer development and correlate with poor prognosis and survival in patients.[57,58] In HCC, DAP3 promotes proliferation, migration and invasion in vitro and in vivo by enhancing mitochondrial respiration, inducing the EMT, and inhibiting cellular senescence. Mechanistically, DAP3 increases the activity of mitochondrial complex I in HCC cells by regulating the translation and expression of MT-ND5.[59] S-phase kinase associated protein 2 (SKP2), a member of F-box protein family, is implicated in tumor initiation, development, and metastasis.[60] For example,

SKP2-mediated transcriptional addiction has been reported to induce anoikis resistance and promote the malignant metastasis in triple-negative breast cancer.[61] In HCC cells, SKP2 expression levels correlate positively with cell proliferation and microvascularization, and inversely with apoptosis and survival. Accordingly, siRNA-mediated SKP2 knockdown in HCC cells reduces proliferation and the ubiquitination of cell cycle regulators, whereas SKP2 overexpression increased proliferation and reduces the expression of cell cycle regulators.[62] Cyclin-dependent kinase inhibitor 3 (CDKN3), a key regulator within the cell cycle network, exhibits aberrant expression in a variety of malignancies, including breast,[63] prostate,[64] liver,[65] and esophageal cancers.[66] Notably, an inverse correlation has been observed between CDKN3 expression levels and the pathological stage of tumors. Specifically, in HCC tissues, CDKN3 inhibition enhances clonogenic capacity and chemotherapeutic tolerance relative to control conditions. Mechanistically, CDKN3 knockdown leads to the downregulation of p53 and p21 protein levels, concurrent with the upregulation of AKT serine/threonine kinase 1. These findings suggest that CDKN3 expression may modulate tumor cell survival and influence the sensitivity to therapeutic agents, potentially through the AKT/P53/P21 signaling pathway.[67]

Nomograms are extensively utilized as prognostic tools in oncology and medicine.[49] In this study, we developed a Nomogram incorporating RS, gender, age, grade, and T_stage to enhance the predictive capacity of ANRGs for evaluating HCC prognosis. Our Nomogram effectively illustrated the survival probabilities for individual patients, as validated through various methods, including AUC values, KM analysis and DCA. Analysis using HPA and GEPIA datasets revealed that the mRNA and protein levels of six ANRGs were significantly elevated in tumor tissues of HCC patients, which were further verified by in vitro and in vivo experimental models.

It is important to acknowledge certain limitations in our anoikis-associated prognostic model for HCC. The results presented in this study are based on retrospective analysis and require validation in prospective studies. Future research will focus on elucidating the mechanisms by which ANRGS influence the prognosis of HCC patients, utilizing clinically relevant experimental models.

Conclusion

This study presents a prognostic risk model established using six ANRGs, specially designed to predict the survival outcomes of patients with HCC. Additionally, a Nomogram has been constructed to directly reflect the survival probabilities for individual patients. In summary, our research does offer a promising risk-predictive tool that has the potential to enhance management strategies for HCC patients, as it can assess HCC risk and identify high-risk patients, thereby facilitating the rational allocation of healthcare resources. Next, it can guide clinical decision-making and provide personalized treatment recommendations for HCC patients. Finally, it can provide a research base for subsequent clinical trials.

Data Sharing Statement

The original contributions presented in the study are included in the article and Supplementary Materials. Further inquiry can be directed to the corresponding authors.

Ethics Statement

The animal experimental protocols have been approved by the Animal Experimentation Ethics Committee of Shanghai University of Traditional Chinese Medicine and were conducted in accordance with the "Helsinki" Declaration for the welfare of the laboratory animals.

Our research employed publicly available datasets from the TCGA, ICGC, and HPA, which include data from patients who have already provided informed consent. Since the study relies exclusively on open-source data, researchers are authorized to freely download and utilize these datasets for research purposes and to publish related findings. Consequently, the clinical research ethics committee review board at Shanghai University of Traditional Chinese Medicine has exempted this study from the requirement for ethical approval.

Statement of Arrive

We have adhered to ARRIVE guidelines and uploaded a completed checklist.

Acknowledgments

We would like to acknowledge the TCGA, ICGC, GEPAI, and HPA databases.

Author Contributions

All authors made a significant contribution to the work reported, whether that is in the conception, study design, execution, acquisition of data, analysis and interpretation, or in all these areas; took part in drafting, revising or critically reviewing the article; gave final approval of the version to be published; have agreed on the journal to which the article has been submitted; and agree to be accountable for all aspects of the work.

Funding

This work was supported by grants from National Natural Science Foundation of China (82222074, 82074154), Shuguang Program of Shanghai Education Development Foundation and Shanghai Municipal Education Commission (23SG38), Youth Tip-Top Talent program in Shanghai, High Level Key Discipline of the State Administration of Traditional Chinese Medicine (ZYYZDXK-2023060).

Disclosure

All the authors declare that they have no conflicts of interest.

References

1. Sung H, Ferlay J, Siegel RL, et al. Global cancer statistics 2020: GLOBOCAN estimates of incidence and mortality worldwide for 36 cancers in 185 countries. *CA*. 2021;71(3):209–249. doi:10.3322/caac.21660
2. Llovet JM, Kelley RK, Villanueva A, et al. Hepatocellular carcinoma. *Nat Rev Gastroenterol Hepatol*. 2021;7(1):6.
3. Chidambaranathan-Reghupaty S, Fisher PB, Sarkar D. Hepatocellular carcinoma (HCC): epidemiology, etiology and molecular classification. *Adv Cancer Res*. 2021;149:1–61.
4. Johnson P, Zhou Q, Dao DY, et al. Circulating biomarkers in the diagnosis and management of hepatocellular carcinoma. *Nat Rev Gastroenterol Hepatol*. 2022;19(10):670–681. doi:10.1038/s41575-022-00620-y
5. Chen Y, Deng X, Li Y, et al. Comprehensive molecular classification predicted microenvironment profiles and therapy response for HCC. *Hepatology*. 2024;80(3):536–551. doi:10.1097/HEP.0000000000000869
6. Wang XH, Fu YL, Xu YN, et al. Ginsenoside Rh1 regulates the immune microenvironment of hepatocellular carcinoma via the glucocorticoid receptor. *J Integr Med*. 2024;22(6):709–718. doi:10.1016/j.joim.2024.09.004
7. Wu J, Liu W, Qiu X, et al. A noninvasive approach to evaluate tumor immune microenvironment and predict outcomes in hepatocellular carcinoma. *Phenomics*. 2023;3(6):549–564. doi:10.1007/s43657-023-00136-8
8. Deng M, Sun S, Zhao R, et al. The pyroptosis-related gene signature predicts prognosis and indicates immune activity in hepatocellular carcinoma. *Mol Med*. 2022;28(1):16. doi:10.1186/s10020-022-00445-0
9. Peng X, Zhu J, Liu S, et al. Signature construction and molecular subtype identification based on cuproptosis-related genes to predict the prognosis and immune activity of patients with hepatocellular carcinoma. *Front Immunol*. 2022;13:990790. doi:10.3389/fimmu.2022.990790
10. Wang Z, Chen X, Zhang J, et al. Based on disulfidptosis-related glycolytic genes to construct a signature for predicting prognosis and immune infiltration analysis of hepatocellular carcinoma. *Front Immunol*. 2023;14:1204338. doi:10.3389/fimmu.2023.1204338
11. Ma Z, Chen M, Liu XL, et al. Identification and verification of a prognostic autophagy-related gene signature in hepatocellular carcinoma. *Sci Rep*. 2024;14(1):3032. doi:10.1038/s41598-024-53565-4
12. Taddei ML, Giannoni E, Fiaschi T, et al. Anoikis: an emerging hallmark in health and diseases. *J Pathol*. 2012;226(2):380–393. doi:10.1002/path.3000
13. Paoli P, Giannoni E, Chiarugi P. Anoikis molecular pathways and its role in cancer progression. *BBA*. 2013;1833(12):3481–3498. doi:10.1016/j.bbamcr.2013.06.026
14. Simpson CD, Anyiwe K, Schimmer AD. Anoikis resistance and tumor metastasis. *Cancer Lett*. 2008;272(2):177–185. doi:10.1016/j.canlet.2008.05.029
15. Wang Y, Fleishman JS, Wang J, et al. Pharmacologically inducing anoikis offers novel therapeutic opportunities in hepatocellular carcinoma. *Biomed Pharmacother*. 2024;176:116878. doi:10.1016/j.biopha.2024.116878
16. Wang Y, Cheng S, Fleishman JS, et al. Targeting anoikis resistance as a strategy for cancer therapy. *Drug Resist Updates*. 2024;75:101099. doi:10.1016/j.drup.2024.101099
17. Guizhen Z, Weiwei Z, Yun W, et al. An anoikis-based signature for predicting prognosis in hepatocellular carcinoma with machine learning. *Front Pharmacol*. 2023;13:1096472. doi:10.3389/fphar.2022.1096472
18. Chen Y, Huang W, Ouyang J, et al. Identification of anoikis-related subgroups and prognosis model in liver hepatocellular carcinoma. *Int J Mol Sci*. 2023;24(3):2862. doi:10.3390/ijms24032862
19. Xiong C, Pan G, Wang H, et al. Construction of an anoikis–related prognostic signature to predict immunotherapeutic response and prognosis in hepatocellular carcinoma. *J Cancer Res Clin Oncol*. 2023;149(18):16869–16884. doi:10.1007/s00432-023-05428-0
20. Zhong Z, Xie F, Yin J, et al. Development of a prognostic model for anoikis and identifies hub genes in hepatocellular carcinoma. *Sci Rep*. 2023;13(1):14723. doi:10.1038/s41598-023-41139-9

21. Weinstein JN, Collisson EA, Mills GB, et al. The cancer genome atlas pan-cancer analysis project. *Nature Genet*. 2013;45(10):1113–1120. doi:10.1038/ng.2764
22. Chen S, Gu J, Zhang Q, Hu Y, Ge Y. Development of biomarker signatures associated with anoikis to predict prognosis in endometrial carcinoma patients. *J Oncol*. 2021;2021:3375297. doi:10.1155/2021/3375297
23. Tang Z, Li C, Kang B, Gao G, Li C, Zhang Z. GEPIA: a web server for cancer and normal gene expression profiling and interactive analyses. *Nucleic Acids Res*. 2017;45(W1):W98–w102. doi:10.1093/nar/gkx247
24. Uhlén M, Fagerberg L, Hallström BM, et al. Proteomics. Tissue-based map of the human proteome. *Science*. 2015;347(6220):1260419. doi:10.1126/science.1260419
25. Yu Z, Guo J, Liu Y, et al. Nano delivery of simvastatin targets liver sinusoidal endothelial cells to remodel tumor microenvironment for hepatocellular carcinoma. *J Nanobiotechnol*. 2022;20(1):9. doi:10.1186/s12951-021-01205-8
26. Vogel A, Meyer T, Sapisochin G, Salem R, Saborowski A. Hepatocellular carcinoma. *Lancet*. 2022;400(10360):1345–1362. doi:10.1016/S0140-6736(22)01200-4
27. Zhong X, Rescorla FJ. Cell surface adhesion molecules and adhesion-initiated signaling: understanding of anoikis resistance mechanisms and therapeutic opportunities. *Cell Signal*. 2012;24(2):393–401. doi:10.1016/j.cellsig.2011.10.005
28. Guadamillas MC, Cerezo A, Del Pozo MA. Overcoming anoikis–pathways to anchorage-independent growth in cancer. *J Cell Sci*. 2011;124(19):3189–3197. doi:10.1242/jcs.072165
29. Fu Y, Wei X, Han Q, et al. Identification and characterization of a 25-lncRNA prognostic signature for early recurrence in hepatocellular carcinoma. *BMC Cancer*. 2021;21(1):1165. doi:10.1186/s12885-021-08827-z
30. Chen Y, Lin Q, Xu Y, et al. An anoikis-related gene signature predicts prognosis and reveals immune infiltration in hepatocellular carcinoma. *Front Oncol*. 2023;13:1158605. doi:10.3389/fonc.2023.1158605
31. Pang M, Sun X, He T, et al. Development of a prognostic model based on anoikis-related genes for predicting clinical prognosis and immunotherapy of hepatocellular carcinoma. *Aging*. 2023;15(19):10253. doi:10.18632/aging.205073
32. Yu X, Feng B, Wu J, et al. A novel anoikis-related gene signature can predict the prognosis of hepatocarcinoma patients. *Transl Cancer Res*. 2024;13(4):1834. doi:10.21037/tcr-23-2096
33. Yu Z, Huang L, Guo J. Anti-stromal nanotherapeutics for hepatocellular carcinoma. *J Control Release*. 2024;367:500–514. doi:10.1016/j.jconrel.2024.01.050
34. Sun L, Su Y, Jiao A, et al. T cells in health and disease. *Sig Transduct Targ Ther*. 2023;8(1):235. doi:10.1038/s41392-023-01471-y
35. Speiser DE, Chijioke O, Schaeuble K, et al. CD4+ T cells in cancer. *Nat Cancer*. 2023;4(3):317–329[EB/OL]. doi:10.1038/s43018-023-00521-2
36. Yang Y, Guo J, Huang L. Tackling TAMs for cancer immunotherapy: it's nano time. *Trends Pharmacol Sci*. 2020;41(10):701–714. doi:10.1016/j.tips.2020.08.003
37. Xu Z, Peng B, Liang Q, et al. Construction of a ferroptosis-related nine-lncRNA signature for predicting prognosis and immune response in hepatocellular carcinoma. *Front Immunol*. 2021;12:719175. doi:10.3389/fimmu.2021.719175
38. Zhang Y, Zou J, Chen R. An M0 macrophage-related prognostic model for hepatocellular carcinoma. *BMC Cancer*. 2022;22(1):791. doi:10.1186/s12885-022-09872-y
39. Goswami S, Anandhan S, Raychaudhuri D, et al. Myeloid cell-targeted therapies for solid tumours. *Nat Rev Immunol*. 2023;23(2):106–120. doi:10.1038/s41577-022-00737-w
40. Gutiérrez-Melo N, Baumjohann D. T follicular helper cells in cancer. *Trends Cancer*. 2023;9(4):309–325. doi:10.1016/j.trecan.2022.12.007
41. Gu-Trantien C, Loi S, Garaud S, et al. CD4+ follicular helper T cell infiltration predicts breast cancer survival. *J Clin Invest*. 2013;123(7):2873–2892. doi:10.1172/JCI67428
42. Lu J, Kang X, Wang Z, Zhao G, Jiang B. The activity level of follicular helper T cells in the peripheral blood of osteosarcoma patients is associated with poor prognosis. *Bioengineered*. 2022;13(2):3751–3759. doi:10.1080/21655979.2022.2031387
43. Bouter A, Carmeille R, Gounou C, et al. Annexin-A5 and cell membrane repair. *Placenta*. 2015;36:S43–S49. doi:10.1016/j.placenta.2015.01.193
44. Hein T, Krammer PH, Weyd H. Molecular analysis of annexin expression in cancer. *BMC Cancer*. 2022;22(1):994. doi:10.1186/s12885-022-10075-8
45. Mui L, Martin CM, Tschirhart BJ, et al. Therapeutic potential of annexins in sepsis and COVID-19. *Front Pharmacol*. 2021;12:735472. doi:10.3389/fphar.2021.735472
46. Wang X, Dai Y, Zhang J, et al. Annexin A5 suppression promotes the progression of cervical cancer. *Arch Gynecol Obstetrics*. 2023;307(3):937–943. doi:10.1007/s00404-022-06524-1
47. Sun X, Wei B, Liu S, et al. Anxa5 mediates the in vitro malignant behaviours of murine hepatocarcinoma Hca-F cells with high lymph node metastasis potential preferentially via ERK2/p-ERK2/c-Jun/pc-Jun (Ser73) and E-cadherin. *Biomed Pharmacother*. 2016;84:645–654. doi:10.1016/j.biopha.2016.09.086
48. Wang W, Liu D, Yao J, et al. ANXA5: a key regulator of immune cell infiltration in hepatocellular carcinoma. *Med Sci Monit*. 2024;30:e943523–1. doi:10.12659/MSM.943523
49. Li F, Aljahdali I, Ling X. Cancer therapeutics using survivin BIRC5 as a target: what can we do after over two decades of study?. *J Exp Clin Cancer Res*. 2019;38(1):368. doi:10.1186/s13046-019-1362-1
50. Fäldt Beding A, Larsson P, Helou K, Einbeigi Z, Parris TZ. Pan-cancer analysis identifies BIRC5 as a prognostic biomarker. *BMC Cancer*. 2022;22(1):322. doi:10.1186/s12885-022-09371-0
51. Dimitrov-Markov S, Perales-Patón J, Bockorny B, et al. Discovery of new targets to control metastasis in pancreatic cancer by single-cell transcriptomics analysis of circulating tumor cells. *Mol Cancer Ther*. 2020;19(8):1751–1760. doi:10.1158/1535-7163.MCT-19-1166
52. Ayoub AM, Mahmoud EAB, Mohamed RH, et al. BIRC5 as a master regulator in HCC: unraveling its role in tumor survival and therapeutic potential. *Funct Integrat Genomics*. 2025;25(1):120. doi:10.1007/s10142-025-01615-z
53. Guindolet D, Gabison EE. Role of CD147 (EMMPRIN/Basigin) in tissue remodeling. *Anat Record*. 2020;303(6):1584–1589. doi:10.1002/ar.24089
54. Gao C, Lu CH, Chen J. Biological characteristics of cluster of differentiation 147 and its relationship with tumour. *Zhongguo Yi Xue Ke Xue Yuan Xue Bao*. 2016;38(5):589–593. doi:10.3881/j.issn.1000-503X.2016.05.018
55. Ma Y, Sun W, Zhang Q, et al. lncRNA BSG-AS1 is hypoxia-responsive and promotes hepatocellular carcinoma by enhancing BSG mRNA stability. *Biochem Biophys Res Commun*. 2021;566:101–107. doi:10.1016/j.bbrc.2021.06.002

56. Kim HR, Chae HJ, Thomas M, et al. Mammalian dap3 is an essential gene required for mitochondrial homeostasis in vivo and contributing to the extrinsic pathway for apoptosis. *FASEB J*. 2007;21(1):188–196. doi:10.1096/fj.06-6283com
57. Sato Y, Yoshino H, Kashiwakura I, Tsuruga E. DAP3 is involved in modulation of cellular radiation response by RIG-I-like receptor agonist in human lung adenocarcinoma cells. *Int J Mol Sci*. 2021;22(1):420. doi:10.3390/ijms22010420
58. Tan S, Zhang X, Guo X, et al. DAP3 promotes mitochondrial activity and tumour progression in hepatocellular carcinoma by regulating MT-ND5 expression. *Cell Death Dis*. 2024;15(7):540. doi:10.1038/s41419-024-06912-2
59. Sui L, Ye L, Sanders AJ, et al. Expression of death associated proteins DAP1 and DAP3 in human pancreatic cancer. *Anticancer Res*. 2021;41 (5):2357–2362. doi:10.21873/anticanres.15010
60. Cai Z, Moten A, Peng D, et al. The Skp2 pathway: a critical target for cancer therapy. *Semi Cancer Biol*. 2020;67(Pt 2):16–33. doi:10.1016/j. semcancer.2020.01.013
61. Li CL, Huang CW, Ko CJ, et al. Curcumol suppresses triple-negative breast cancer metastasis by attenuating anoikis resistance via inhibition of Skp2-mediated transcriptional addiction. *Anticancer Res*. 2020;40(10):5529–5538. doi:10.21873/anticanres.14565
62. Calvisi DF, Ladu S, Pinna F, et al. SKP2 and CKS1 promote degradation of cell cycle regulators and are associated with hepatocellular carcinoma prognosis. *Gastroenterology*. 2009;137(5):1816–1826.e10. doi:10.1053/j.gastro.2009.08.005
63. Qi L, Zhou B, Chen J, et al. Significant prognostic values of differentially expressed-aberrantly methylated hub genes in breast cancer. *J Cancer*. 2019;10(26):6618–6634. doi:10.7150/jca.33433
64. Gu P, Yang D, Zhu J, Zhang M, He X. Bioinformatics analysis identified hub genes in prostate cancer tumorigenesis and metastasis. *Math Biosci Eng*. 2021;18(4):3180–3196. doi:10.3934/mbe.2021158
65. Jiang CH, Yuan X, Li JF, et al. Bioinformatics-based screening of key genes for transformation of liver cirrhosis to hepatocellular carcinoma. *J Transl Med*. 2020;18(1):40. doi:10.1186/s12967-020-02229-8
66. Wang W, Liao K, Guo HC, et al. Integrated transcriptomics explored the cancer-promoting genes CDKN3 in esophageal squamous cell cancer. *J Cardiothorac Surg*. 2021;16(1):148. doi:10.1186/s13019-021-01534-7
67. Dai W, Fang S, Cai G, et al. CDKN3 expression predicates poor prognosis and regulates Adriamycin sensitivity in hepatocellular carcinoma in vitro. *J Int Med Res*. 2020;48(7):0300060520936879. doi:10.1177/0300060520936879